Expansion Methods for Medical Imaging

Habib Ammari

Department of Mathematics and Applications, Ecole Normale Supérieure, Paris

Expansion Methods

- Add structural information or supply missing information to determine specific features with satisfactory resolution and stability.
- Expansion methods used for:
  - scale separations: small targets (potential tumors at early stage), small wave attenuation, small sound speed fluctuations.
  - reconstructions of internal energies in multi-physics imaging from small internal changes in the medium.
- Expansion methods $\Rightarrow$ inversion and optimal design methodologies: analytically investigate the robustness with respect to incomplete data, measurement and medium noises.

Expansion Methods

Small size targets:

- Anomaly detection:
  - boundary and scattering measurements
- Distribution of physical parameters:
  - boundary measurements from internal perturbations of the medium
  - internal measurements

Expansion Methods

Expansion types:

- Boundary Measurements: outer expansions in terms of the characteristic size of the anomaly
  - anomaly detection
- Internal Measurements: inner expansions
  - distribution of physical parameters

Plan

- Conductivity problem: outer expansions, inner expansions, super-resolved imaging.
- Frequency-domain imaging: compare different imaging functionals.
- Time-domain imaging: time reversal methods, corrections of the effects of attenuation in the medium and random fluctuations in wave speed.
- Applications of Expansion Methods in multi-physics imaging.
- Concluding remarks.

Conductivity Problem

Notation: $\Omega \in \mathbb{R}^d (d \geq 2)$: smooth bounded domain.
$N(x,z)$: Neumann function for $-\Delta$ in Ω corresponding to a Dirac mass at $z \in \Omega$:

$$\begin{cases} -\Delta_x N(x,z) = \delta_z \quad \text{in } \Omega \ , \\ \dfrac{\partial N}{\partial \nu_x}\Big|_{\partial\Omega} = -\dfrac{1}{|\partial\Omega|} \ , \displaystyle\int_{\partial\Omega} N(x,z)\, d\sigma(x) = 0 \ . \end{cases}$$

B: smooth bounded domain. $\hat{v}$: corrector the solution to

$$\begin{cases} \Delta\hat{v} = 0 \quad \text{in } \mathbb{R}^d \setminus \overline{B} \ , \quad \Delta\hat{v} = 0 \quad \text{in } B \ , \\ \hat{v}|_- - \hat{v}|_+ = 0 \quad \text{on } \partial B \ , \quad k\dfrac{\partial\hat{v}}{\partial\nu}|_- - \dfrac{\partial\hat{v}}{\partial\nu}|_+ = 0 \quad \text{on } \partial B \ , \\ \hat{v}(\xi) - \xi \to 0 \quad \text{as } |\xi| \to +\infty \ . \end{cases}$$

Conductivity Problem

$D = \delta B + z$: anomaly $\subset \Omega$; δ: characteristic size of the anomaly; conductivity $0 < k \neq 1 < +\infty$.

The voltage potential u:

$$\begin{cases} \nabla \cdot \Big(\chi(\Omega \setminus \overline{D}) + k\chi(D) \Big) \nabla u = 0 \quad \text{in } \Omega \ , \\ \left. \dfrac{\partial u}{\partial \nu} \right|_{\partial\Omega} = g \quad \left(g \in L^2(\partial\Omega), \displaystyle\int_{\partial\Omega} g \, d\sigma = 0 \right) \ , \\ \displaystyle\int_{\partial\Omega} u \, d\sigma = 0 \ . \end{cases}$$

U: the background solution.

Outer Expansion

- Dipole-type approximation of the conductivity anomaly.
- **Theorem:** [Friedman-Vogelius] Outer expansion for $d = 2, 3$:

$$(u - U)(x) \approx -\delta^d \nabla U(z) M(k, B) \nabla_z N(x, z) \quad \text{on } \partial\Omega.$$

- $M(k, B) := (k - 1) \int_B \nabla \hat{v}(\xi)\, d\xi$: the first-order polarization tensor (PT)
- The location z and the matrix $M(k, B)$: reconstructed.
- $M(k, B)$: - characterizes all the information about the anomaly that can be learned from boundary measurements.
  - mixture of k and low-frequency geometric information.
- Canonical correspondence between ellipses (ellipsoids) and PTs.
- (with Kang, Lecture Notes Math., Springer 2004.)

Polarization Tensor

- Properties of the polarization tensor:

  (i) M is symmetric.

  (ii) If $k > 1$, then M is positive definite, and it is negative definite if $0 < k < 1$.

  (iii) Hashin-Shtrikman bounds:

$$\begin{cases} \dfrac{1}{k-1}\,\mathrm{trace}(M) \leq (d-1+\dfrac{1}{k})|B|\ , \\ (k-1)\,\mathrm{trace}(M^{-1}) \leq \dfrac{d-1+k}{|B|}\ . \end{cases}$$

- Optimal size estimates; Thickness estimates; Pólya–Szegö conjecture.
- Lipton, Capdeboscq-Vogelius, Capdeboscq-Kang, Kang-Milton.

Polarization Tensor

Visualization of PT

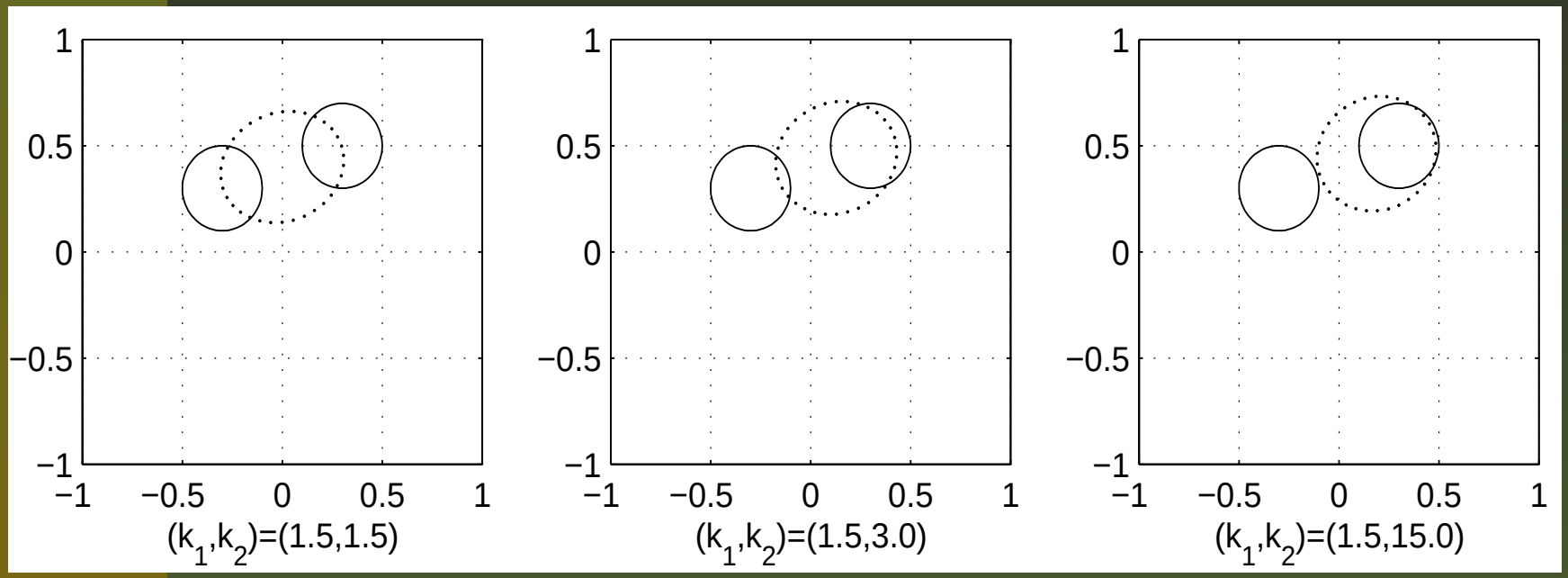

Figure 1: When the two disks have the same radius and the conductivity of the one on the right-hand side is increasing, the equivalent ellipse is moving toward the right anomaly.

Polarization Tensor

Visualization of PT

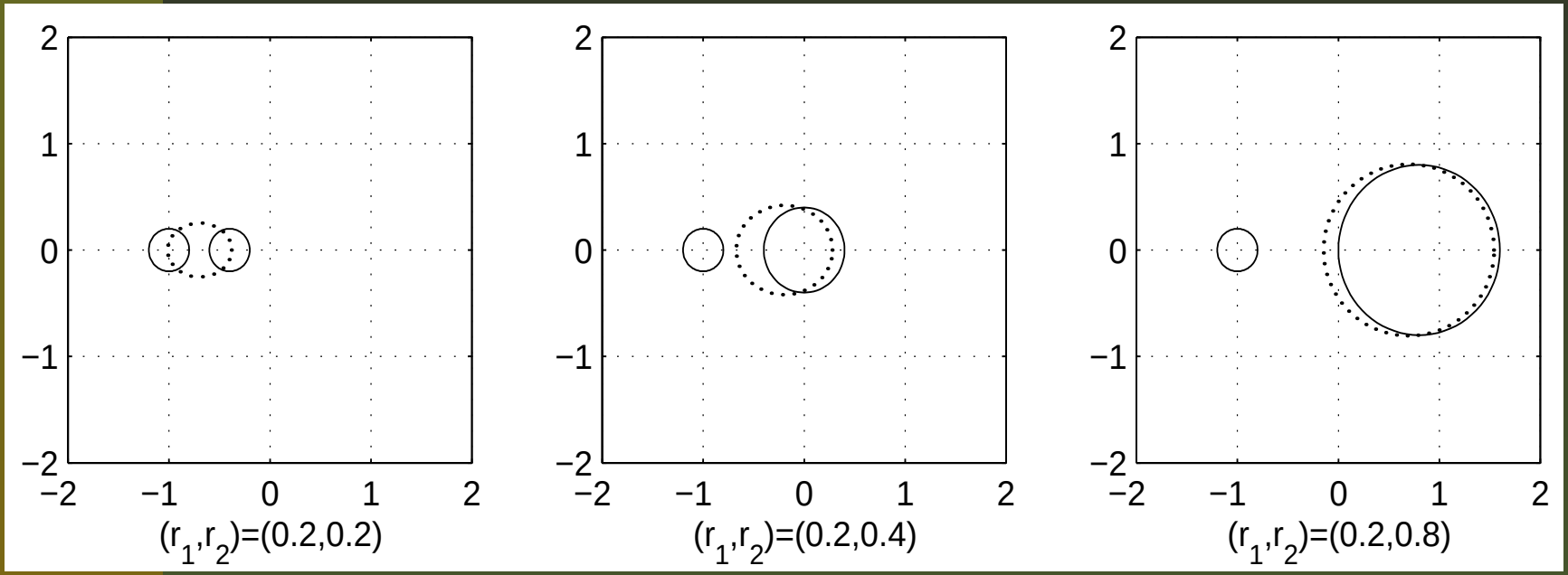

Figure 2: When the conductivities of the two disks is the same and the radius of the disk on the right-hand side is increasing, the equivalent ellipse is moving toward the right anomaly.

High-Order Polarization Tensors

- **Theorem:** Higher order asymptotic expansion for $x \in \partial\Omega$ (multipolar expansion)

$$u(x) = U(x)$$
$$+ \sum_\alpha \sum_\beta \frac{(-1)^{|\beta|}\delta^{|\alpha|+|\beta|}}{\alpha!\beta!} \partial^\alpha U(z) M_{\alpha\beta}(k, B) \partial^\beta N(x, z) + O(\delta^{2d}).$$

- $M_{\alpha\beta}(k, B)$: generalized polarization tensors (GPTs).
- A complete asymptotic expansion is possible. Terms higher than δ^{2d-1} involves not only GPTs but also the boundary-inclusion interaction.
- $M_{\alpha\beta}(k, B)$ can be obtained from boundary measurements.

High-Order Polarization Tensors

Properties of the GPTs

- Symmetry: If $\{a_\alpha\}$ and $\{b_\beta\}$ are such that $\sum a_\alpha x^\alpha$ and $\sum b_\beta x^\beta$ are harmonic polynomials, then

$$\sum a_\alpha b_\beta M_{\alpha\beta} = \sum a_\alpha b_\beta M_{\beta\alpha}$$

- Positivity: If $k > 1$, then

$$\sum a_\alpha a_\beta M_{\alpha\beta} > 0.$$

- Unique determination of D by GPTs: If

$$\sum a_\alpha b_\beta M_{\alpha\beta}(k_1, B_1) = \sum a_\alpha b_\beta M_{\alpha\beta}(k_2, B_2) \quad \forall a_\alpha, b_\beta,$$

then $k_1 = k_2$ and $B_1 = B_2$.

High-Order Polarization Tensors

- The harmonic moments of B can be estimated from the GPTs.
- Wiener-type bounds: Let $k > 1$ and $f = \sum_\alpha a_\alpha x^\alpha$ be a harmonic polynomial. Then

$$(1 - \frac{1}{k}) \int_B |\nabla f|^2 \leq \sum a_\alpha a_\beta M_{\alpha\beta}(k, B) \leq (k-1) \int_B |\nabla f|^2.$$

- (with H. Kang, *Polarization and Moment Tensors*, Springer 2007).

High-Order Polarization Tensors

- (with H. Kang, M. Lim, and H. Zribi, Math. Comp. 2011).
- Make use of $\sum_{|\alpha|+|\beta|\leq K} a_\alpha b_\beta M_{\alpha\beta}$ for a fixed $K \geq 2$ to image finer details of the shape of the inclusion and separate material parameter/geometry.
- Hopping algorithm in $|\alpha| + |\beta|$ for finding fine shape details from GPTs: if B is the target domain, minimize over B'

$$\sum_{|\alpha|+|\beta|\leq K} w_{|\alpha|+|\beta|} \left| \sum_{\alpha,\beta} a_\alpha b_\beta M_{\alpha\beta}(k, B') - \sum_{\alpha,\beta} a_\alpha b_\beta M_{\alpha\beta}(k, B) \right|^2$$

- $w_{|\alpha|+|\beta|}$ are binary weights: $w_{|\alpha|+|\beta|} = 1$(on) or 0(off).
- A good choice for the initial guess: the equivalent ellipse.

High-Order Polarization Tensors

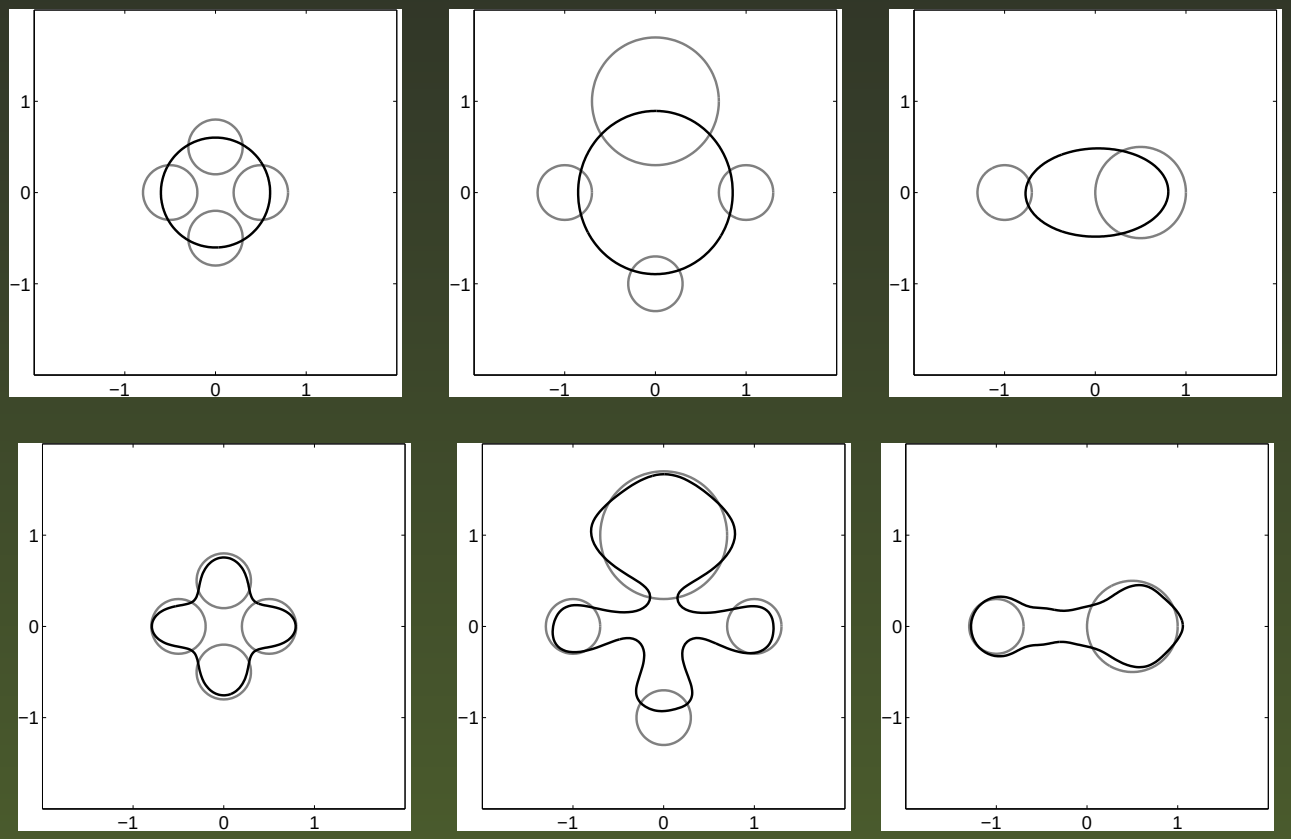

Figure 3: Reconstruction of clusters of inclusions. The upper images: the equivalent ellipses, and the lower ones: results after $K = 6$ iterations.

High-Order Polarization Tensors

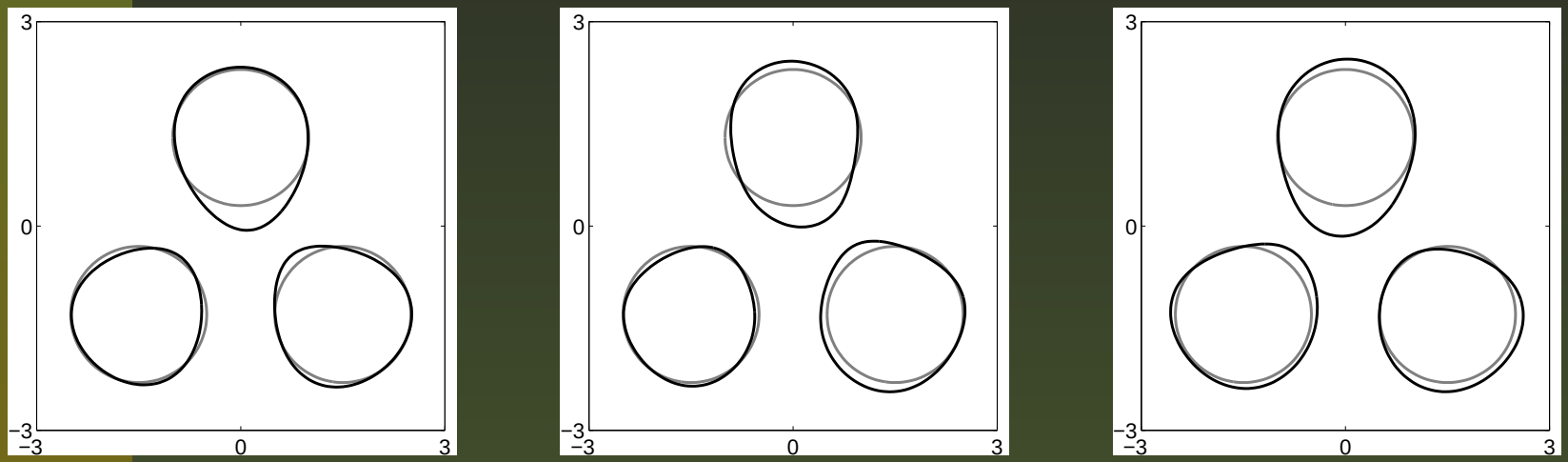

Figure 4: Reconstructions from noisy data using a level set formulation (S. Yu).

Inner Expansion

Theorem: The following inner asymptotic formula holds:

$$u(x) \approx U(z) + \delta \hat{v}(\frac{x-z}{\delta}) \cdot \nabla U(z) \quad \text{for } x \text{ near } z \ .$$

- Boundary independent reconstruction: no need of an exact knowledge of the boundary of the domain Ω
- Local reconstruction
- Separate conductivity/ geometry
- Interface approximation: high frequency information
- Trade off between resolution and stability

Internal Measurements

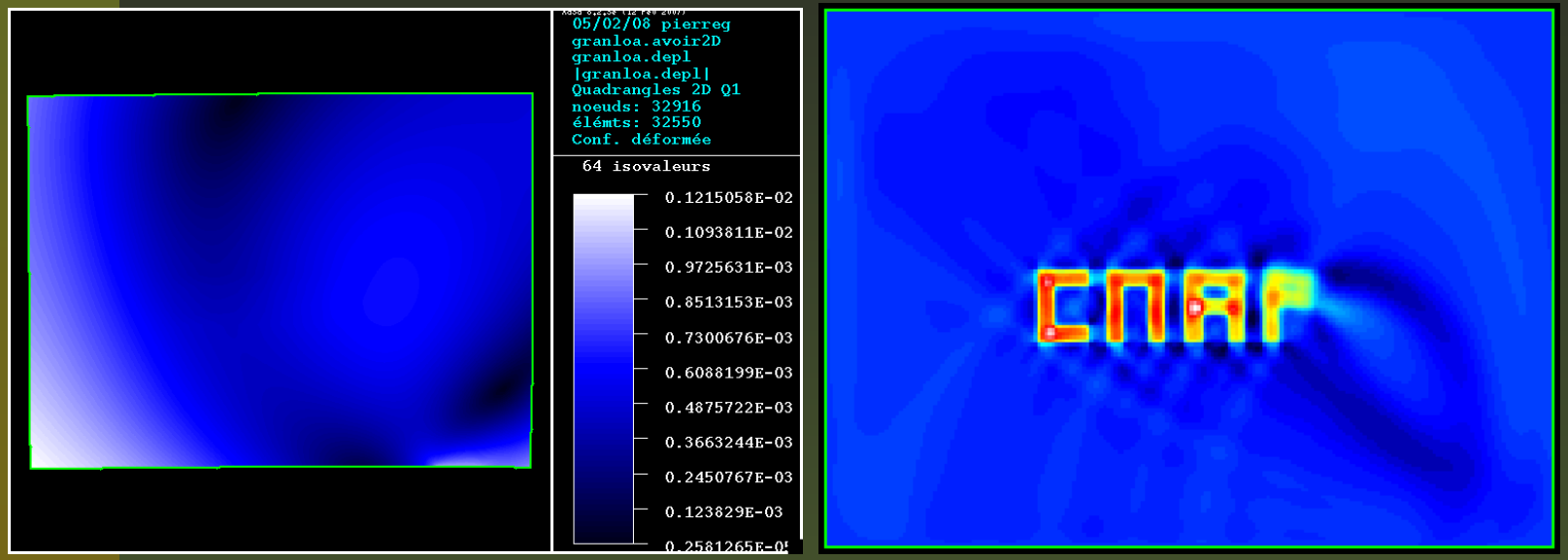

Figure 5: Reconstruction from internal measurements.

Internal Measurements

Minimization of the discrepancy functional: trade off between resolution and stability:

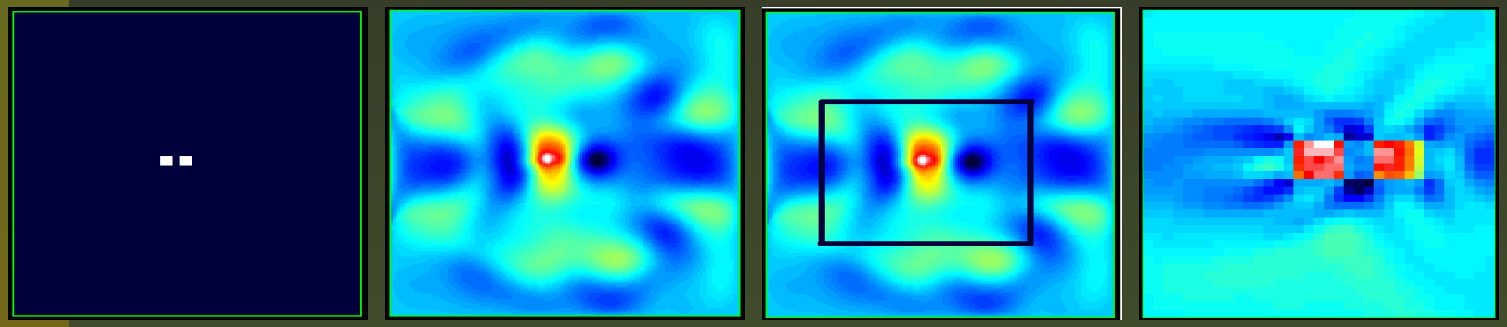

Frequency-Domain Imaging

- Reconstruction algorithms and shape representations in wave imaging: dependence on the wavelength $2\pi/\omega$, the Signal-to-noise ration (SNR), and the distance to the target.
- Size of the target compared to the wavelength: small.
- Far-field measurements.
- SNR of an imaging functional $\mathcal{I}$:

$$\mathrm{SNR}(\mathcal{I}) = \frac{\mathbb{E}[\mathcal{I}(z,\omega)]}{\mathrm{Var}(\mathcal{I}(z,\omega))^{1/2}},$$

z the location of the inclusion.

Frequency-Domain Imaging

- ω: frequency; μ_0, ϵ_0: magnetic permeability, electrical permittivity of the background.
- μ, ϵ: those of the target D.
- $\Gamma^\omega(x)$ be the outgoing Green function for $\Delta + \omega^2$ in $\mathbb{R}^d$.
- Put $k_0 = \omega\sqrt{\epsilon_0\mu_0}$ and $k = \omega\sqrt{\epsilon\mu}$.
- Incident field: $U(x) = \Gamma^{k_0}(x - y)$.
- Total field: the solution to

$$\nabla \cdot (\tfrac{1}{\mu_0}\chi(\mathbb{R}^d \setminus D) + \tfrac{1}{\mu}\chi(D))\nabla u(\cdot, y) \\ +\omega^2(\epsilon_0\chi(\mathbb{R}^d \setminus D) + \epsilon\chi(D))u(\cdot, y) = \tfrac{1}{\mu_0}\delta_y$$

with the radiation condition imposed on u.

Frequency-Domain Imaging

- Transmitter and receiver arrays: $\{y_1, \ldots, y_N\}$.
- The multi-static response (MSR) matrix:

$$\big(u(y_i, y_j) - \Gamma^{k_0}(y_i, y_j)\big)_{i,j=1,\ldots,N}.$$

- Reciprocity property $\longrightarrow$ MSR complex symmetric in the absence of noise (but not Hermitian).
- The imaging problem: to reconstruct the target D and μ, ϵ from the MSR matrix at a single or multiple frequencies.

Frequency-Domain Imaging

- **Theorem:** Multipolar asymptotic expansion: $D = \delta B + z$, x: measurement point; y: source point.

$$(u-U)(x) = \delta^{d-2} \sum_{p=0}^{\infty} \delta^p \sum_{|\alpha|+|\beta|=p} \frac{1}{\alpha!\beta!} W_{\alpha\beta} \partial_z^\alpha \Gamma^{k_0}(z,y) \partial_z^\beta \Gamma^{k_0}(x,z)$$

- $W_{\alpha\beta}$ depends on k, k_0, and δ: frequency-dependent polarization tensor (FDPT).
- $\lim_{\delta\to 0} W_{\alpha\beta}$ for $|\alpha| + |\beta| \leq 1 \to$ leading-order term (Vogelius-Volkov)

$$k_0^2 (\frac{\epsilon}{\epsilon_0} - 1)|B|\Gamma^{k_0}(z,y)\Gamma^{k_0}(x,z) + M\nabla_z \Gamma^{k_0}(z,y) \cdot \nabla_z \Gamma^{k_0}(x,z).$$

- M: polarization tensor.

Frequency-Domain Imaging

- **Proposition**–Structure of MSR matrix:

$$A_{ij} := u(y_i, y_j) - \Gamma^{k_0}(y_i, y_j) \approx \mathcal{G}(y_i, z)\mathcal{W}\mathcal{G}(y_j, z)^T,$$

- Row vector $\mathcal{G}(y_i, z)$:

$$\mathcal{G}(y_i, z) = \left(\partial_z^\alpha \Gamma^{k_0}(y_i, z)\right)_{|\alpha| \le n}.$$

(size $(n+1)(n+2)/2$ in $d = 2$; $(n+1)(n+2)(n+3)/6$ in $d = 3$)

- Matrix $\mathcal{W}$:

$$\mathcal{W} = \left(\frac{\delta^{d-2+|\alpha|+|\beta|}}{\alpha!\beta!} W_{\alpha\beta}\right)_{|\alpha|,|\beta| \le n}.$$

SVD Structure

- SVD of the MSR matrix:

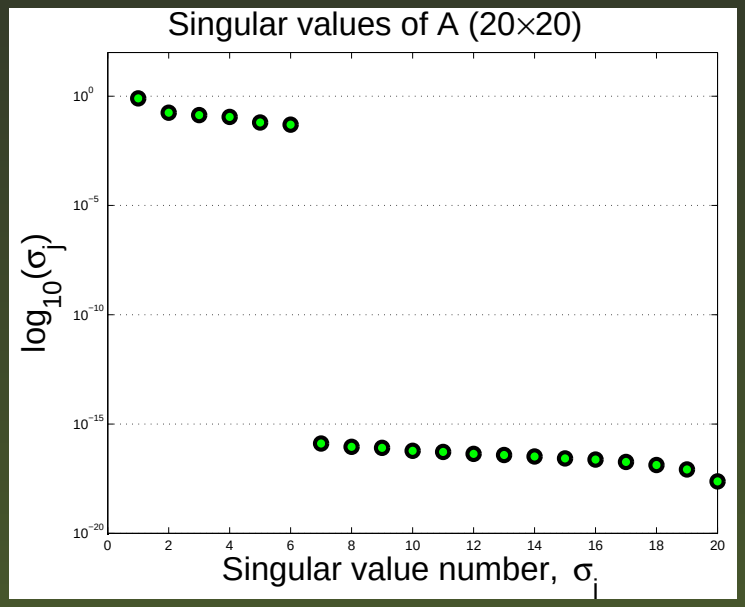

Figure 6: Singular value decomposition of the response matrix **A** corresponding to two well-separated inclusions of general shape for $N = 20$, using a standard log scale. Six singular values emerge from the 14 others in the noise subspace.

SVD Structure

Extended targets: direct imaging not possible. Optimal control approach is efficient.

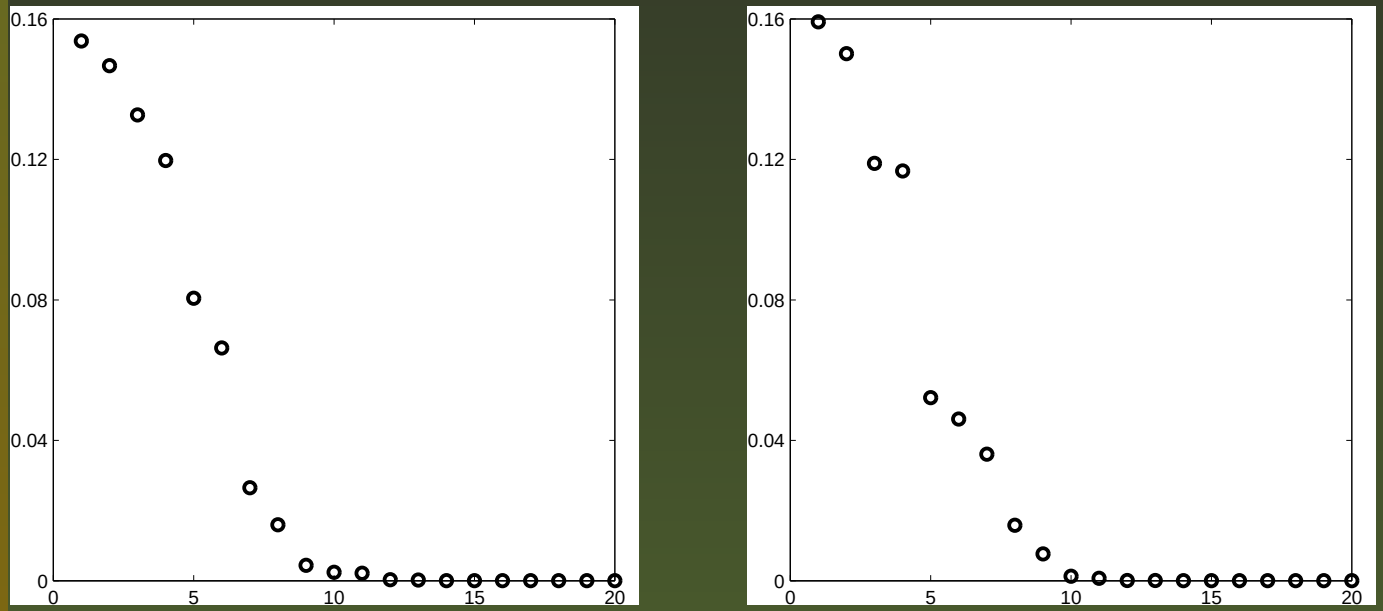

Figure 7: Singular values of the MSR matrix with 20 transmitters and 20 receivers. The number of significant singular values is about 10 out of 20. Left: unit disk centered at the origin; Right: general shaped target.

Frequency-Domain Imaging

Localization procedure:

- To locale the target:
  - Backpropagation (also called Reverse-Time Migration): P_m orthogonal projection onto the m first eigenvectors of MSR matrix,

$$\mathcal{I}_{BP}(z^s) := \frac{\displaystyle\sum_{|\alpha|\leq 1} \|(I - P_m)(\partial^\alpha \Gamma^{k_0}(\cdot, z^s))\|}{\displaystyle\sum_{|\alpha|\leq 1} \|P_m(\partial^\alpha \Gamma^{k_0}(\cdot, z^s))\|}.$$

  - Kirchhoff migration $\mathcal{I}_{KM}$, MUSIC $\mathcal{I}_{MU}$ or topological derivative based imaging functional $\mathcal{I}_{TD}$.

Imaging Functionals

- $\mathcal{I}_{KM}, \mathcal{I}_{MU}$: subspace weighted projection algorithms.
- Nonlinear relation between $\mathcal{I}_{KM}$ and $\mathcal{I}_{MU}$: $\mathcal{I}_{KM} \sim 1/(1 - \mathcal{I}_{MU}^2)$.
- $\mathcal{I}_{TD}$: sensitivity of a misfit function relative to the insertion of an inclusion at $\mathbf{z}^S$. Maximum$\rightarrow$ point at which the insertion of an inclusion centered at that point maximally decreases the misfit function.
- $\mathcal{I}_{TD}$: backpropagation of the error term in a coherent way.
- $\mathcal{I}_{BP}, \mathcal{I}_{KM}, \mathcal{I}_{MU}, \mathcal{I}_{TD}$: large peaks only at the locations of the inclusions.
- Formulas for the SNR: $\mathrm{SNR}(\mathcal{I}_{\mathrm{KM}}) =$ volume $\times\omega\times$ contrast $/$ standard deviation of the noise.

Imaging Functionals

- Stability: Backpropagation is the most robust with respect to measurement noise.
- Resolution: $n = 1 \rightarrow$ classical resolution limit.
- Resolution: $n > 1 \rightarrow$ super-resolved imaging if one modifies appropriately the imaging functional (in the regime $\delta \ll \mathrm{dist} \ll \lambda = 2\pi/k_0$).
- Modified imaging functional:

$$\mathcal{I}_{BP}^{(n)}(z^s) := \frac{\displaystyle\sum_{|\alpha|=n} \|(I - P_m)(\partial^\alpha \Gamma^{k_0}(\cdot, z^s))\|}{\displaystyle\sum_{|\alpha|=n} \|P_m(\partial^\alpha \Gamma^{k_0}(\cdot, z^s))\|}.$$

Backpropagation-Type Imaging

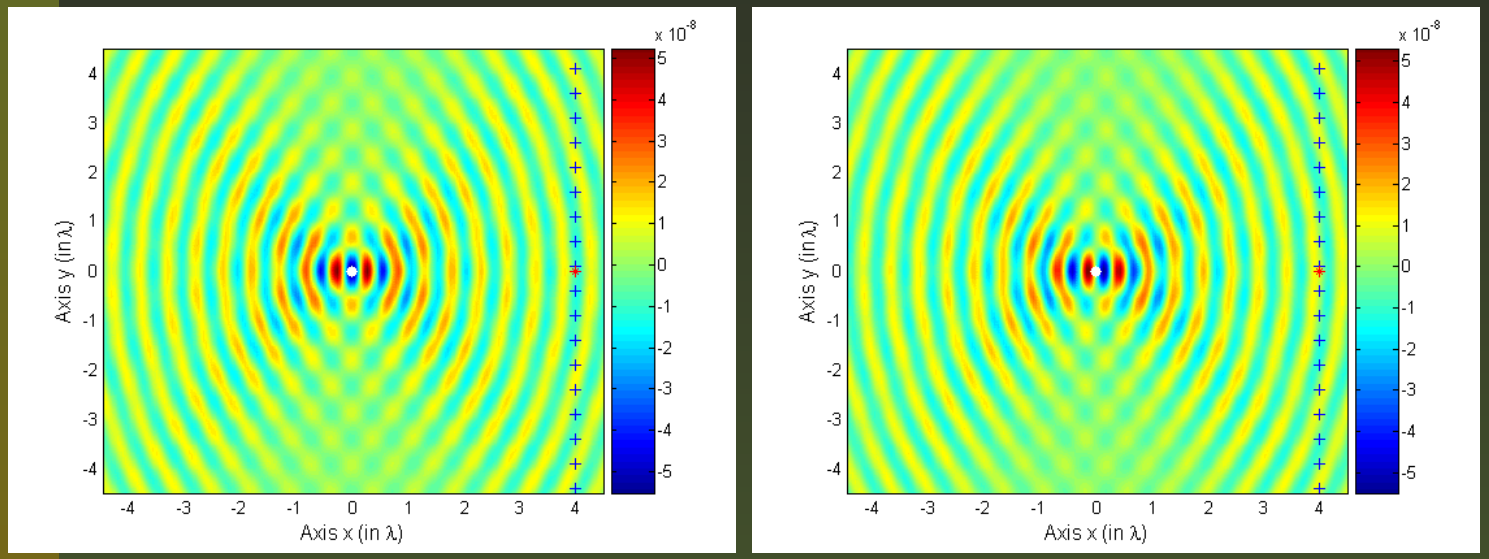

Figure 8: Real and imagery part of the BP imaging functional. Here ’*’ and ’+’ respectively show the transceiver and the receiver positions.

MUSIC-Type Imaging

- MUSIC Imaging functional:

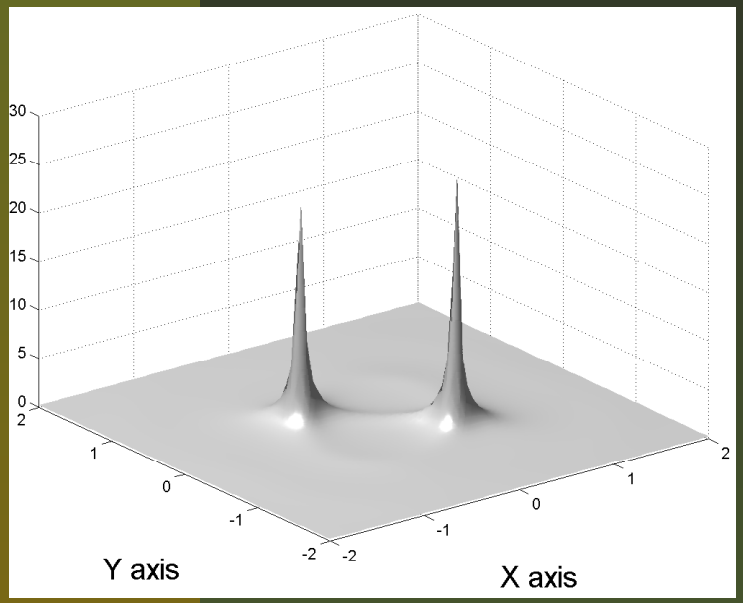

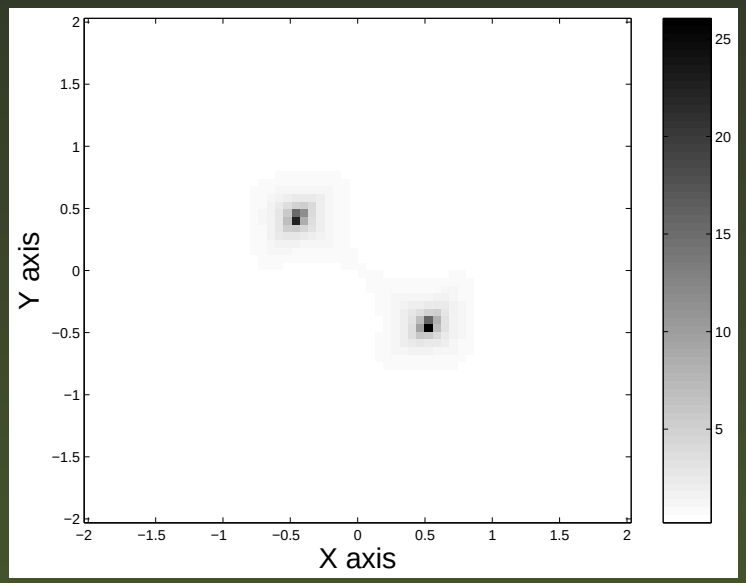

Figure 9: MUSIC-type reconstruction from the singular value decomposition of $\mathbf{A}$ represented in Figure 6.

Imaging Functionals

- Multi-frequency data: summing over frequencies improve imaging via higher effective SNR if independent identically distributed noises.
- Correlation between measurements: single-frequency imaging or Coherent interferometry strategy (CINT) [Borcea-Garnier-Papanicolaou-Tsogka].

Imaging Functionals

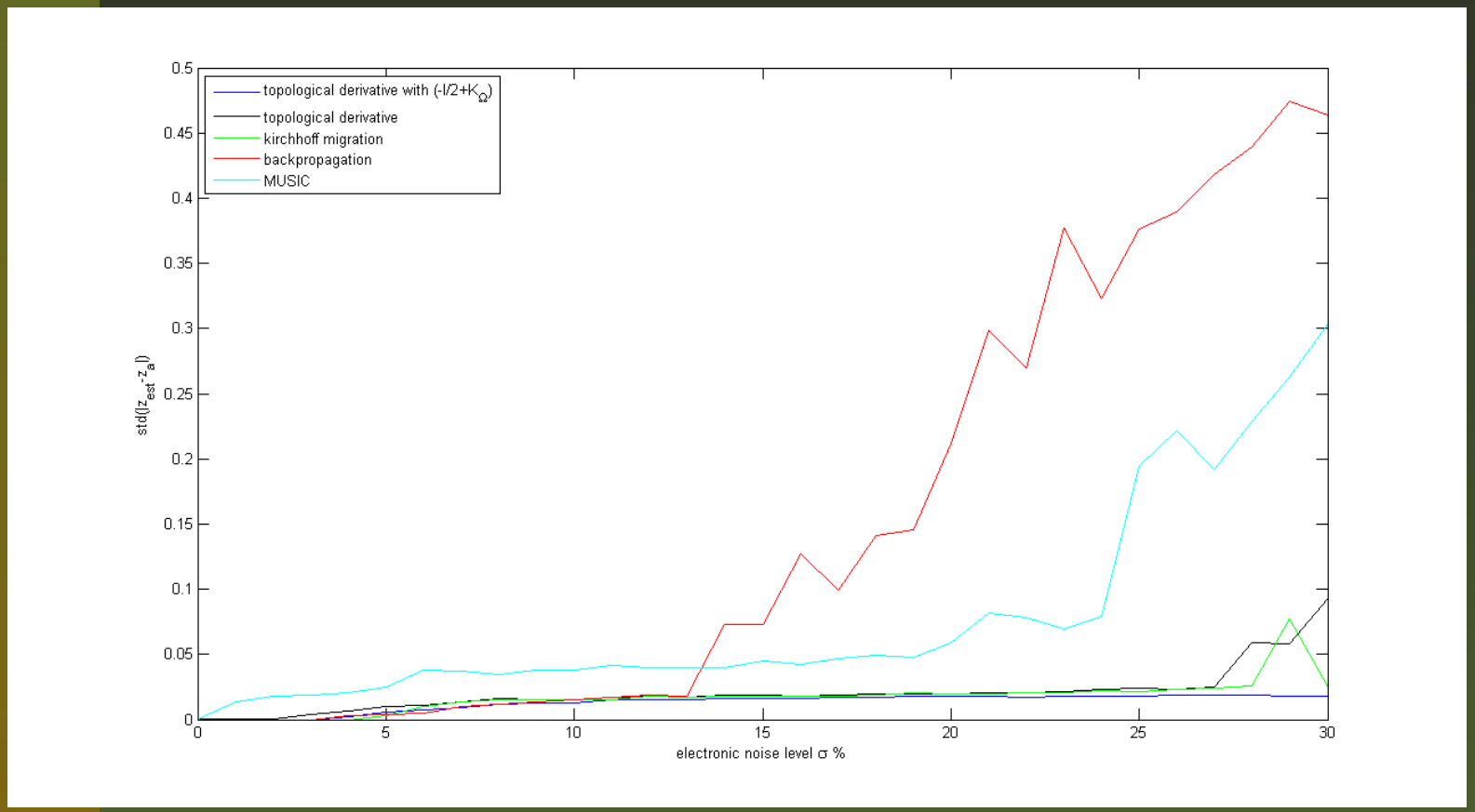

Figure 10: Standard deviations of localization error with respect to electronic noise level for $\mathcal{I}_{\mathrm{MU}}, \mathcal{I}_{\mathrm{BP}}, \mathcal{I}_{\mathrm{KM}}$, and $\mathcal{I}_{\mathrm{TD}}$.

Imaging Functionals

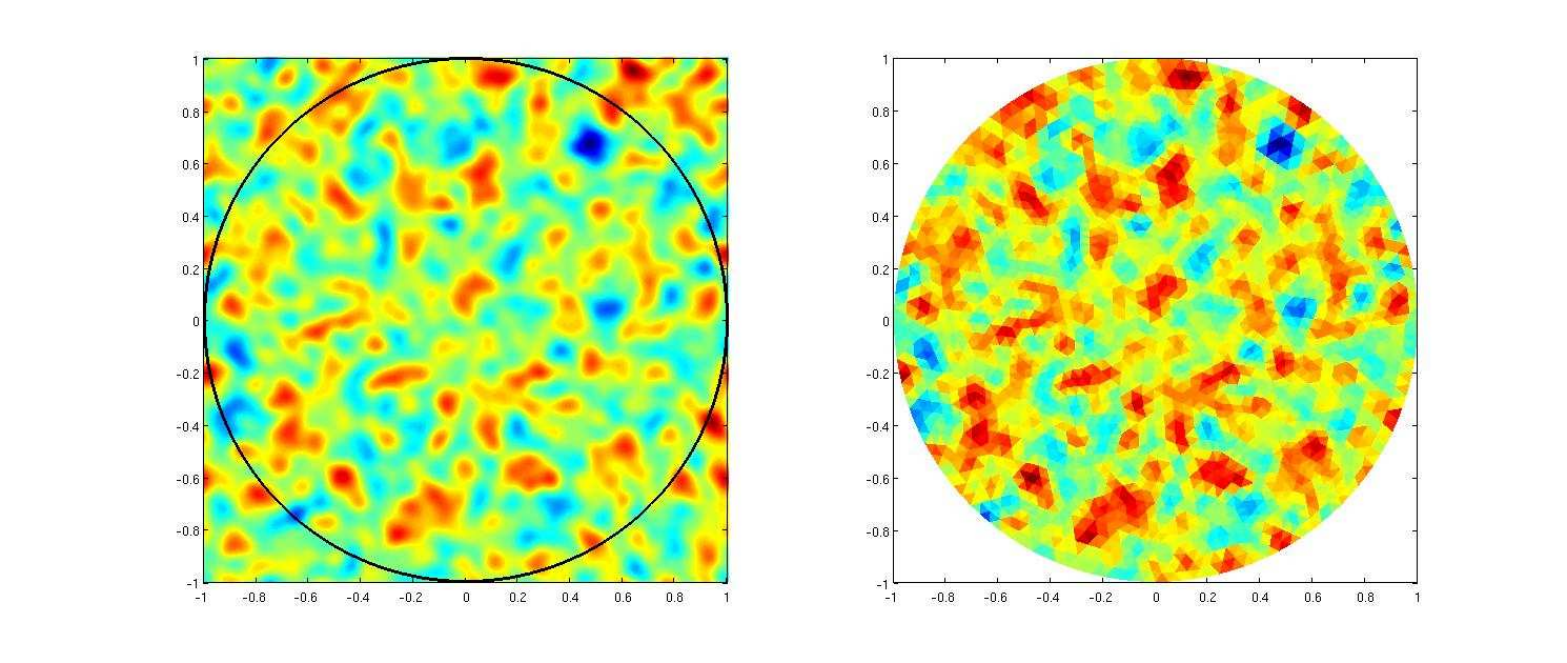

Figure 11: Realization of a medium noise.

Imaging Functionals

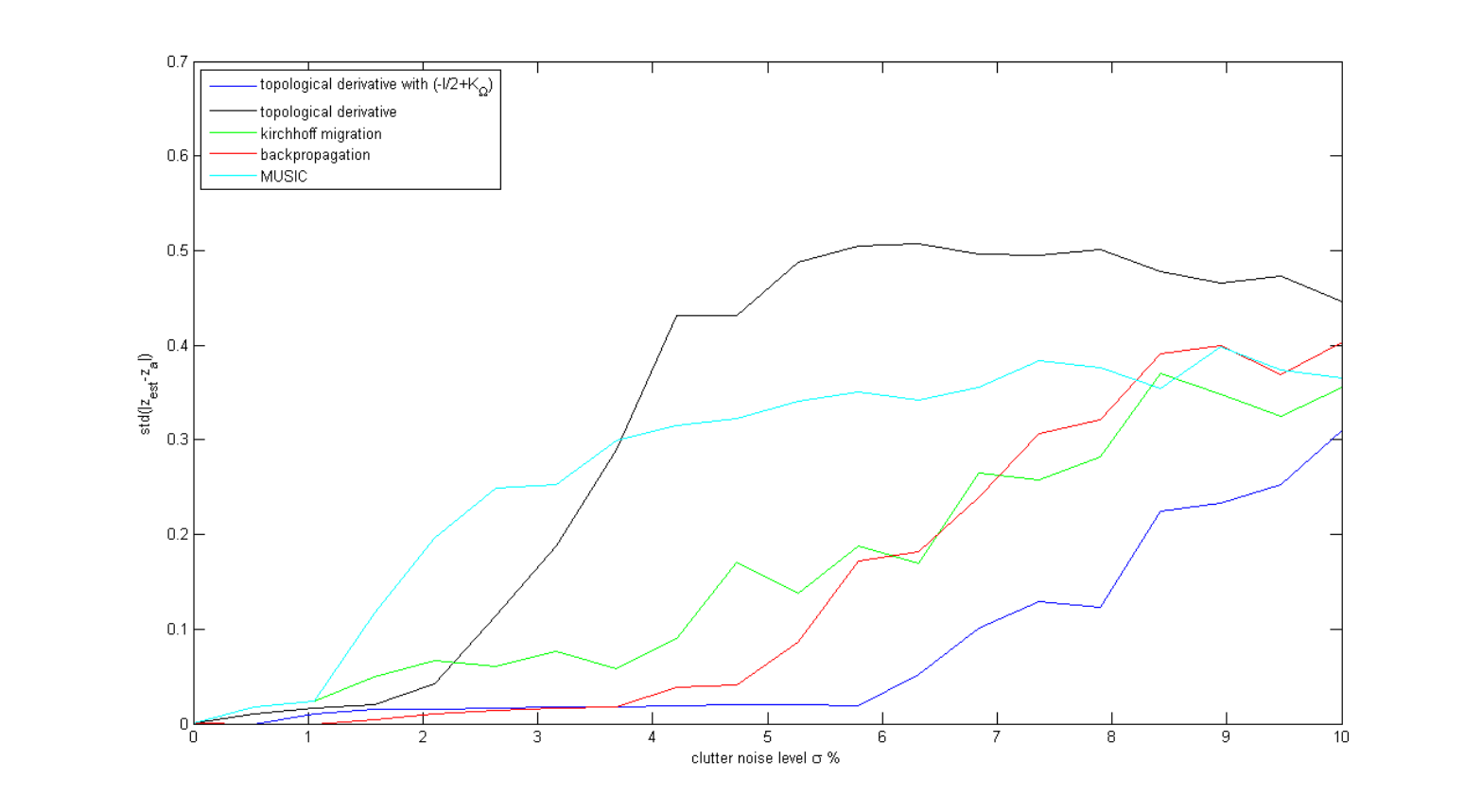

Figure 12: Standard deviations of localization error with respect to clutter noise for $\mathcal{I}_{\mathrm{MU}}, \mathcal{I}_{\mathrm{BP}}, \mathcal{I}_{\mathrm{KM}}$, and $\mathcal{I}_{\mathrm{TD}}$.

Time-Domain Imaging

- (with P. Garapon, L. Guadarrama Bustos, and H. Kang, JDE 10)
- $U_y(x,t)$ retarded Green's function generated at $y \in \Omega$ and $t = 0$ without the anomaly.
- The wave in the presence of the anomaly:

$$\begin{cases} \partial_t^2 u - \nabla \cdot \big(\chi(\mathbb{R}^3 \setminus \overline{D}) + k\chi(D)\big)\nabla u = \delta_{x=y}\delta_{t=0}, \mathbb{R}^3 \times]0, +\infty[, \\ u(x,t) = 0 \quad \text{for} \quad x \in \mathbb{R}^3 \quad \text{and } t \ll 0. \end{cases}$$

- Truncate the high-frequency component of the signal up to $\rho = O(\delta^{-\alpha}), \alpha < 1$,

$$P_\rho[u](x,t) = \int_{|\omega| \le \rho} e^{-i\omega t} \hat{u}(x,\omega) d\omega.$$

Time-Domain Imaging

- $T = |y - z|$ travel time between the source and the anomaly.
- After truncation of the high frequency component, the perturbation due to the anomaly is (approximately) a wave emitted from the point z at $t = T$.
- Truncation parameter ρ up to $O(\delta^{-\alpha}), \alpha < 1$.
- Far field expansion of $P_\rho[u - U_y](x,t)$:

$$= -\delta^3 \int_{\mathbb{R}} \nabla P_\rho[U_z](x, t-\tau) \cdot M(k,B) \nabla P_\rho[U_y](z,\tau)\, d\tau$$
$$+ O(\delta^{4(1-\frac{3}{4}\alpha)}).$$

- The anomaly behaves then like a dipolar source.

Time-Reversal Imaging

- To detect the anomaly from far-field measurements one can use a time-reversal technique.
- One measures the perturbation on a closed surface surrounding the anomaly, truncates its high-frequency component, and retransmits it through the background medium in a time-reversed chronology.
- The perturbation will travel back to the location of the anomaly.

Time-Reversal Imaging

- The reversed wave (after high-frequency truncation)

$$w_{\text{tr}}(x,t) = \int_{\mathbb{R}} ds \int_{\partial\Omega} \Big[U_x(x',t-s) \frac{\partial P_\rho[u-U_y]}{\partial \nu}(x',t_0-s) - \frac{\partial U_x}{\partial \nu}(x',t-s) P_\rho[u-U_y](x',t_0-s) \Big] \, d\sigma(x').$$

- $(p := M(k,B)\nabla P_\rho[U_y](z,T))$

$$w_{\text{tr}}(x,t) \approx -\delta^3 p \cdot \nabla_z \big[P_\rho[U_z](x,t_0-T-t) - P_\rho[U_z](x,t-t_0+T) \big].$$

- The reversed wave is the sum of incoming and outgoing spherical waves.

Time-Reversal Imaging

- Frequency domain (Γ^ω outgoing Green's function):

$$\int_{\partial\Omega}\left[\Gamma^\omega(x-x')\overline{\frac{\partial\Gamma^\omega}{\partial\nu}(z-x')}-\overline{\Gamma^\omega}(z-x')\frac{\partial\Gamma^\omega}{\partial\nu}(x-x')\right]d\sigma(x')$$
$$=2i\Im m\,\Gamma^\omega(z-x)\ (\text{ resolution limit in imaging}).$$

- Inhomogeneous media: similar Helmholtz-Kirchhoff identity.
- Resolution limit: size of the focal spot of order half the wavelength.
- Sharper the behavior of $\Im m\,\Gamma^\omega$ at z, higher the resolution.
- Super-resolution: dependence of $\Im m\,\Gamma^\omega$ on the heterogeneity of the medium ? Local change of the medium around the inclusion.
- (with E. Bonnetier and Y. Capdeboscq, SIAP 09)

Time Reversal Imaging

- (with E. Bretin, J. Garnier, A. Wahab, CONM 11)
- Reconstruct the source term $f(x)$ from $g(x,t) := u(x,t)$ on $\partial\Omega \times [0,T]$,

$$\begin{cases} \partial_t^2 u(x,t) - \Delta u(x,t) = 0, \quad (x,t) \in \mathbb{R}^d \times [0,T] \\ u(x,0) = f(x), \quad \partial_t u(x,0) = 0. \end{cases}$$

- G Dirichlet Green function:

$$\begin{cases} \dfrac{\partial^2 G}{\partial t^2}(x,y,\tau,t) - \Delta_y G(x,y,\tau,t) = \delta_x \delta_\tau, \quad (y,t) \in \Omega \times \mathbb{R}, \\ G(x,y,\tau,t) = 0, \quad \dfrac{\partial G}{\partial t}(x,y,\tau,t) = 0, \quad t \ll \tau, \\ G(x,y,\tau,t) = 0, \quad (y,t) \in \partial\Omega \times \mathbb{R}. \end{cases}$$

Time Reversal Imaging

- Exact time reversal:

$$f(x) = \int_0^T \int_{\partial\Omega} \frac{\partial G(x,y,T,t)}{\partial \nu_y} g(y,t-T) d\sigma(y) \quad \forall x \in \Omega.$$

- Modified time reversal: Helmholtz-Kirchhoff identity $\Rightarrow$ use of the free-space Green function U_x:

$$f(x) \simeq \int_0^T \int_{\partial\Omega} \frac{\partial U_x}{\partial t}(y,s,t) g(y,T-s)\, d\sigma(y)\, ds.$$

Attenuation

- Correct the attenuation effect.
- Thermo-viscous model:

$$\begin{cases} \partial_t^2 u_a(x,t) - \Delta u_a(x,t) - a\partial_t(\Delta u_a(x,t)) = 0 \\ u_a(x,0) = f(x), \quad \text{and} \quad \partial_t u_a(x,0) = 0. \end{cases}$$

- Attenuation breaks time-reversibility of the wave equation.
- Classical time-reversal produces blurring in reconstructing source terms.
- Regularize the time reversed attenuated wave equation: truncate high frequencies in time or in space.
- Reconstruct the ideal data in the unattenuated medium and then apply classical time-reversal.

Attenuation

- $\widetilde{\Gamma}_{a,\omega}$: free space fundamental solution of the Helmholtz equation

$$\omega^2 \widetilde{\Gamma}_{a,\omega}(x,y) + (1 + ia\omega)\, \Delta \widetilde{\Gamma}_{a,\omega}(x,y) = -\delta_x \quad \text{in } \mathbb{R}^d.$$

- Regularized free space fundamental solution:

$$\widetilde{\Gamma}_{a,\rho}(x,y,s,t) = \frac{1}{2\pi} \int_{|\omega| \le \rho} \widetilde{\Gamma}_{a,\omega}(x,y) e^{-i\omega(t-s)} d\omega.$$

- Regularized time reversal:

$$\mathcal{I}_{2,a,\rho}(x) = \int_{\partial\Omega} \int_0^T \frac{\partial}{\partial t} \widetilde{\Gamma}_{a,\rho}(x,y,s,T) g_a(y, T-s) d\sigma(y) ds.$$

Attenuation

- Relationship between u_a and u:

$$u_a(x,t) = \mathcal{L}_a[u(x,.)](t);$$

$$\mathcal{L}_a[\phi](t) = \frac{1}{2\pi}\int \frac{\kappa(\omega)}{\omega}\left\{\int \phi(s)e^{i\kappa(\omega)s}ds\right\}e^{-i\omega t}d\omega.$$

- $\kappa(\omega) = \dfrac{\omega}{\sqrt{1-ia\omega}}.$
- Obtain the ideal data g from g_a: $\mathcal{L}$ is not well conditioned.

Attenuation

- Regularized inverse of $\mathcal{L}$ via a singular value decomposition (SVD) [La Rivière, Zhang, and Anastasio];
- In physical situations, the coefficient of attenuation a is very small $\Rightarrow$ asymptotic behavior of $\mathcal{L}$ as the attenuation coefficient a tends to zero.
- Stationary Phase Theorem $\Rightarrow$ Asymptotics as $a \longrightarrow 0$:

$$\mathcal{L}_a[\phi](t) = \phi(t) + \frac{a}{2}\left(t\phi'\right)'(t) + o(a).$$

Attenuation

- High-order approximation:

$$\mathcal{L}_a[\phi](t) = \sum_{m=0}^{k} \frac{a^m}{m!\ 2^m} \left(t^m \phi'\right)^{(2m-1)}(t) + o(a^k).$$

- An approximation of order k of the inverse of operator $\mathcal{L}_a$:

$$\mathcal{L}_{a,k}^{-1}\phi = \sum_{m=0}^{k} a^m \phi_{k,m}(t),$$

- $\phi_{k,m}$ recursively defined by

$$\phi_{k,0} = \phi, \qquad \phi_{k,m} = -\sum_{l=1}^{m} \mathcal{D}_l[\phi_{k,m-l}],$$

- $\mathcal{D}_m\phi(t) = \frac{1}{m!\ 2^m}\left(t^m\phi'\right)^{(2m-1)}(t).$

Attenuation

- Step 1: Preprocess the measured data g_a using the filter $\mathcal{L}_{a,k}^{-1}$;
- Step 2: Use the classical time-reversal functional for the reconstruction of the source f.

Time Reversal Imaging

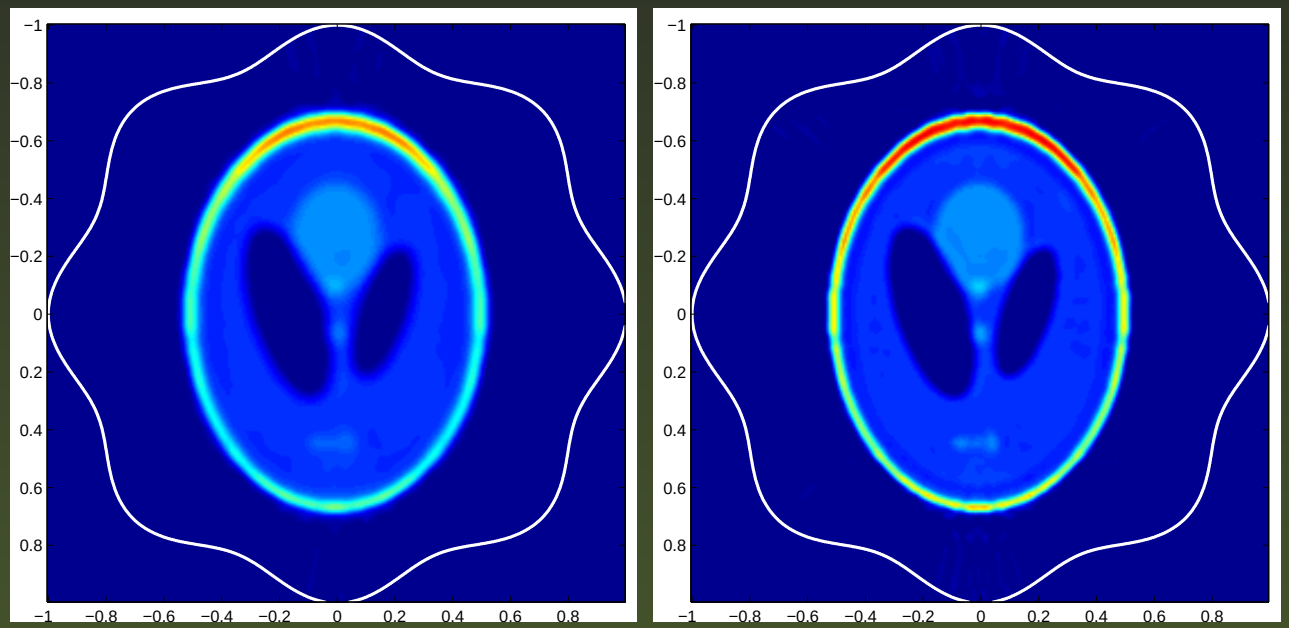

Figure 13: Reconstruction by preprocessing the data with the filter $\mathcal{L}_{a,k}^{-1}$; $a = 0.001$; Left: $k = 1$; Right: $k = 4$.

Attenuation

- Regularized time reversal:

$$\mathcal{I}_{2,a,\rho}(x) = \int_{\partial\Omega}\int_0^T \frac{\partial}{\partial t}\widetilde{\Gamma}_{a,\rho}(x,y,s,T)g_a(y,T-s)d\sigma(y)ds.$$

- Regularized time reversal $\mathcal{I}_{2,a,\rho}$ first order correction of the attenuation effect:

$$\mathcal{I}_{2,a,\rho}(x) = \delta_{\rho,x} * f + o(a),$$

- $\delta_{\rho,x}$: approximation of the Dirac delta distribution.

Attenuation

- Introduce the operator:

$$\widetilde{\mathcal{L}}_{a,\rho}[\phi](t) = \frac{1}{2\pi}\int_0^\infty \phi(s)\left\{\int_{|\omega|\le\rho} \frac{\widetilde{\kappa}(\omega)}{\omega} e^{i\widetilde{\kappa}(\omega)s - i\omega t} d\omega\right\} ds,$$

- $\widetilde{\kappa}(\omega) = \dfrac{\omega}{\sqrt{1+ia\omega}}.$
-

$$\frac{\partial \widetilde{\Gamma}_{a,\rho}}{\partial t} = \widetilde{\mathcal{L}}_{a,\rho}\left[\frac{\partial \Gamma}{\partial t}\right].$$

- Approximate inverse of $\mathcal{L}_a$:

$$\widetilde{\mathcal{L}}^*_{a,\rho}\mathcal{L}_a[\phi] = P_\rho[\phi] + o(a),$$

- P_ρ: truncates high-frequencies.

Cluttered Sound Speed

- (with E. Bretin, J. Garnier, V. Jugnon, SINUM 11)
- Wave equation:

$$\begin{cases} \dfrac{\partial^2 u}{\partial t^2}(x,t) - c(\mathbf{x})^2 \Delta u(x,t) = 0, \\ u(x,0) = f(x), \qquad \dfrac{\partial u}{\partial t}(x,0) = 0. \end{cases}$$

- Unknown cluttered sound speed:

$$\frac{1}{c(x)^2} = 1 + \sigma_c \mu\Big(\frac{x}{x_c}\Big),$$

μ: stationary random process, x_c: correlation length of the fluctuations of $c(x)$, σ_c: their standard deviation.

Cluttered Sound Speed

- Phases of the measured waves $\hat{u}(\omega, \mathbf{y})$ are shifted with respect to the deterministic, unperturbed phase because of the unknown clutter.
- Numerically back-propagated in the homogeneous medium with speed of propagation equal to one: the phase terms do not compensate each other $\Rightarrow$ blurring and loss of resolution.
- Correct the effect of a clutter: pre-process the data and back-propagate the space and frequency correlations between them.
- CINT (Coherent Interferometry)-Radon algorithm/Kirchhoff-Radon migration.
- Original CINT [Borcea, Garnier, Papanicolaou, Tsogka].

Cluttered Sound Speed

- Two dimensions + $\partial\Omega$: unit circle.
- Exact inversion formula [L. Nguyen]:

$$f = \frac{1}{(2\pi)^3} \int_{\partial\Omega} \int_{\mathbb{R}} \widehat{\mathcal{BW}[g]}(y,\omega) e^{-i\omega|x-y|} d\omega d\sigma(y), \quad \mathbf{x} \in \Omega,$$

-

$$\mathcal{W}[g](y,r) := 4r \int_0^r \frac{u(y,t)}{\sqrt{r^2 - t^2}} dt, \quad y \in \partial\Omega, \quad r \in \mathbb{R}^+,$$

- $\mathcal{B}$: filter

$$\mathcal{B}[h](y,t) = \int_0^2 \frac{d^2 h}{dr^2}(\mathbf{y}, r) \ln(|r^2 - t^2|)\, dr, \quad y \in \partial\Omega.$$

Cluttered Sound Speed

- Pre-processed data: $q = \frac{1}{4\pi^2}\mathcal{BW}[g]$.
- Kirchhoff-Radon migration imaging function:

$$\mathcal{I}_{\mathrm{KRM}}(x) = \frac{1}{2\pi}\int_{\partial\Omega} d\sigma(y)\int_{\mathbb{R}} d\omega \hat{q}(x,\omega)e^{-i\omega|x-y|}.$$

- CINT-Radon imaging function:

$$\mathcal{I}_{\mathrm{CIR}}(x) = \frac{1}{(2\pi)^2}\iint_{\partial\Omega\times\partial\Omega} d\sigma(y_1)d\sigma(y_2)$$
$$\times\iint_{\mathbb{R}\times\mathbb{R}} d\omega_1 d\omega_2 e^{-\frac{(\omega_2-\omega_1)^2}{2\Omega_d^2}} e^{-\frac{|y_1-y_2|^2}{2X_d^2}}$$
$$\times\widehat{q}(y_1,\omega_1)e^{-i\omega_1|x-y_1|}\overline{\widehat{q}}(y_2,\omega_2)e^{i\omega_2|x-y_2|}.$$

Cluttered Sound Speed

- CINT-Radon: compute the local correlation of the pre-processed data in a time interval scaled by $1/\Omega_d$ and superpose the back-propagated local correlations over pairs of receivers that are not further apart from X_d.
- CINT-Radon: keep the pairs (y_1, ω_1) and (y_2, ω_2) for which the pre-processed data $\hat{q}(y_1, \omega_1)$ and $\hat{q}(y_2, \omega_2)$ are coherent and remove the pairs that do not bring information.
- If $\Omega_d \to \infty$ and $X_d \to \infty$, then $\mathcal{I}_{\mathrm{CIR}}$ is the square of the Kirchhoff-Radon migration function:

$$\mathcal{I}_{\mathrm{CIR}}(x) = |\mathcal{I}_{\mathrm{KRM}}(x)|^2.$$

Cluttered Sound Speed

- Stability and resolution analysis of CINT-Radon and Kirchhoff-Radon.
- Kirchhoff-Radon: strong damping and very small SNR.
- CINT-Radon: high SNR and choice of the cut-off parameters $\Omega_d \simeq$ frequency coherence radius and $X_d \simeq$ spatial coherence radius achieves a good trade-off between resolution and stability. Smaller values increase SNR but reduces the resolution.
- Optimize over Ω_d and X_d the quality of the image [as in adaptive CINT, Borcea-Papanicolaou-Tsogka].

Cluttered Sound Speed

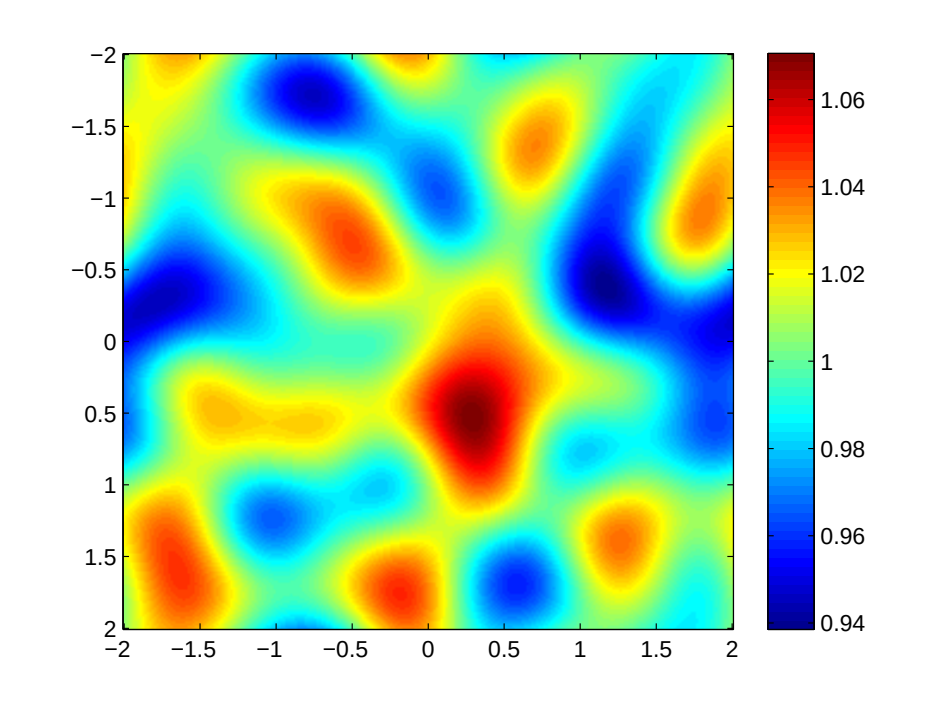

Figure 14: Random velocity.

Cluttered Sound Speed

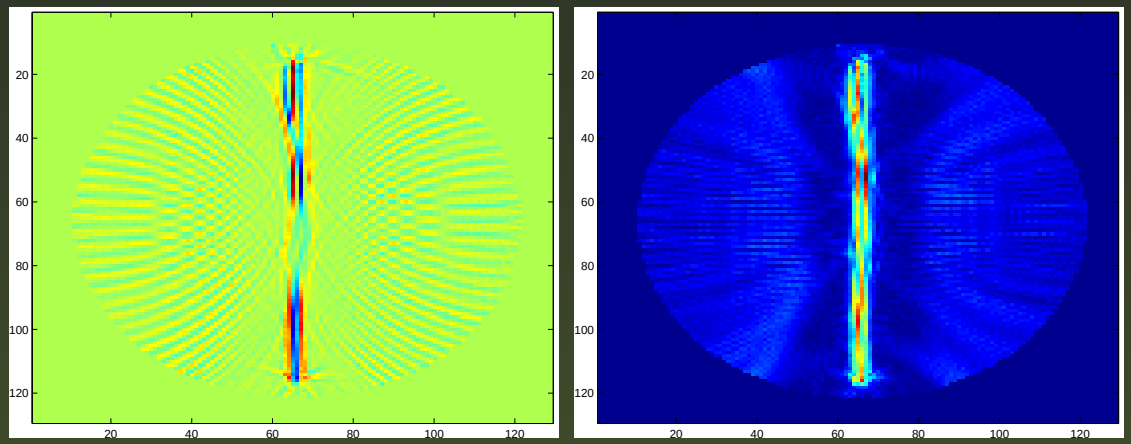

Figure 15: Source reconstructions using $\mathcal{I}_{\mathrm{KRM}}$ (left) and $\mathcal{I}_{\mathrm{CIR}}$, with $X_d = 2$ and $\Omega_d = 200$ (right).

Cluttered Sound Speed

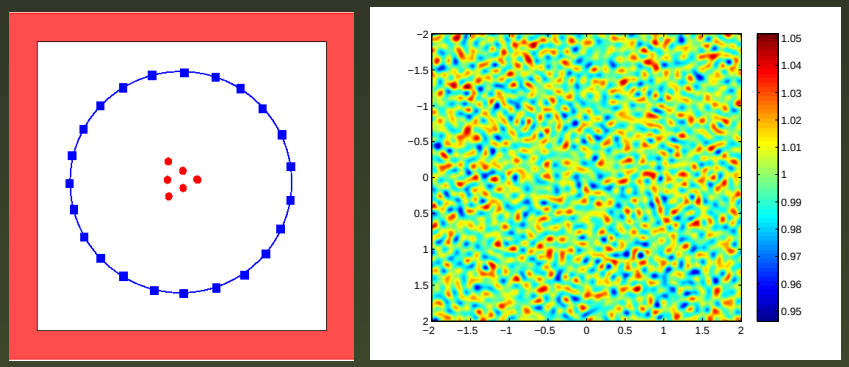

Figure 16: Left: point sources; right: random velocity with high frequencies.

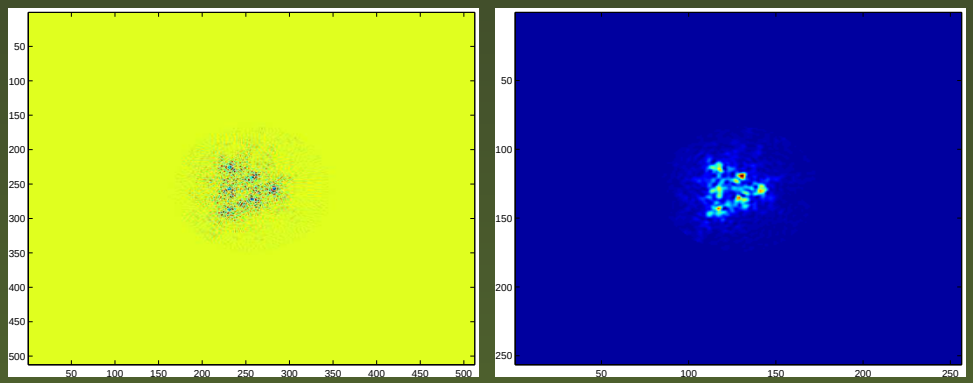

Figure 17: Left: Kirchhoff reconstruction; right: CINT reconstruction.

Multi-physics Imaging

- One single imaging system based on the combined use of two kinds of waves.
- One wave will give its contrast and the second its spatial resolution.
- *An Introduction to Mathematics of Emerging Biomedical Imaging*, Springer, 2008.

Multi-physics Imaging

- (with E. Bonnetier, Y. Capdeboscq, M. Tanter, and M. Fink, SIAP 08)
- u the voltage potential induced by a current g in the absence of acoustic perturbations:

$$\begin{cases} \nabla_x \cdot (\gamma(x)\nabla_x u) = 0 \text{ in } \Omega \ , \\ \gamma(x)\dfrac{\partial u}{\partial \nu} = g \text{ on } \partial\Omega \ , \end{cases}$$

- Suppose γ bounded from below and above and known in a neighborhood of the boundary $\partial\Omega$: $\gamma = \gamma_\star$; Set $\Omega' \subset \Omega$ where γ is unknown.

Multi-physics Imaging

- Use 2 different amplitudes of focalized ultrasonic waves (with the same focal spot D) $\rightarrow$

$$\gamma_\delta(x) \;=\; \gamma(x)\Big[1+\chi(D)(x)\,(\nu(x)-1)\Big],$$

with $\nu(x)$: known.

- u_δ induced by g in the presence of acoustic perturbations localized in the focal spot $D := z + \delta B$:

$$\begin{cases} \nabla_x \cdot (\gamma_\delta(x)\nabla_x u_\delta(x)) = 0 \text{ in } \Omega, \\ \gamma(x)\dfrac{\partial u_\delta}{\partial \nu} = g \text{ on } \partial\Omega. \end{cases}$$

Multi-physics Imaging

- **Theorem:** Suppose the focal spot D to be a disk and $u \in W^{2,\infty}(D)$. Then,

$$\int_{\partial\Omega} (u_\delta - u) g \, d\sigma = |\nabla u(z)|^2 \int_D \gamma(x) \frac{(\nu(x)-1)^2}{\nu(x)+1} dx$$
$$+ O(|D|^{1+\kappa}),$$

  - $O(|D|^{1+\kappa}) \leq C|D|^{1+\kappa} ||\nabla u||_{L^\infty(D)} |\nabla^2 u||_{L^\infty(D)}$ with C: independent of D and u.
  - κ: depends only on Ω', ν, $\sup_\Omega \gamma, \min_\Omega \gamma$.

Multi-physics Imaging

- **Corollary:** Suppose $\gamma \in \mathcal{C}^{0,\alpha}(D)$, $0 \leq \alpha \leq 2\kappa \leq 1$. Then

$$\begin{aligned}\mathcal{E}(z) &:= \left(\int_D \frac{(\nu(x)-1)^2}{\nu(x)+1}dx\right)^{-1} \int_{\partial\Omega}(u_\delta - u)g\,d\sigma \\ &= \gamma(z)\,|\nabla u(z)|^2 + O(|D|^{\alpha/2}).\end{aligned}$$

  - $\mathcal{E}(z)$: known function from the boundary measurements;
  - $\gamma(z)\,|\nabla u(z)|^2$: electrical energy density;
  - Focal spot D not a disk: slightly different approximation for the electrical energy density;
  - $\alpha = 0 \rightarrow$ remainder $o(1)$.

Multi-physics Imaging

- Substitute γ by $\mathcal{E}/\left|\nabla u\right|^2$.
- Nonlinear PDE (the 0–Laplacian)

$$\begin{cases} \nabla_x \cdot \left(\dfrac{\mathcal{E}}{\left|\nabla u\right|^2} \nabla u \right) = 0 \quad \text{in } \Omega \ , \\ \dfrac{\mathcal{E}}{\left|\nabla u\right|^2} \dfrac{\partial u}{\partial \nu} = g \quad \text{on } \partial\Omega \ . \end{cases}$$

- g such that u has no critical point inside Ω'.
- Choose two currents g_1 and g_2 s.t. $\nabla u_1 \times \nabla u_2 \neq 0$ for all $x \in \Omega$.

Multi-physics Imaging

- (with Y. Capdeboscq, F. de Gournay, A. Rozanova, and F. Triki, preprint)
- Model problem: The Helmholtz equation

$$\begin{cases} \nabla \cdot (\gamma \nabla u) + k^2 q u = 0 \text{ in } \Omega, \\ \gamma \dfrac{\partial u}{\partial \nu} = g \text{ on } \partial\Omega. \end{cases}$$

- Reconstruct both γ and q for fixed frequency k (not a resonant frequency).
- Focalized ultrasonic waves: local change in the electromagnetic parameters of the medium γ and q, linearly with respect to the amplitude of the ultrasonic signal.
- Generalize the 0-Laplacian approach.

Multi-physics Imaging

- Use 4 different amplitudes of ultrasonic waves (with the same focal spot) $\rightarrow \gamma_\delta(x) = \gamma(x)\Big[1 + \chi(D)(x)\,(\nu_1(x) - 1)\Big]$, and $q_\delta(x) = q(x)\Big[1 + \chi(D)(x)\,(\nu_2(x) - 1)\Big]$, with $\nu_i(x)$: known.
- **Theorem:** Focal spot D: disk; γ and $q \in \mathcal{C}^{0,\alpha}(D)$, $u \in W^{2,\infty}(D)$;

$$\int_{\partial\Omega}(u_\delta - u)\overline{g}\,d\sigma = \gamma(z)\,|\nabla u(z)|^2 \int_D \frac{(\nu_1(x) - 1)^2}{\nu_1(x) + 1}dx$$
$$+k^2 q(z)|u(z)|^2 \int_D (\nu_2(x) - 1)dx + O(|D|^{1+\alpha/2}).$$

- $\alpha = 0 \rightarrow$ remainder $o(|D|)$.

Multi-physics Imaging

- Obtain $\mathcal{E}_\gamma := \gamma\,|\nabla u|^2$ and $\mathcal{E}_q := q|u|^2$ from boundary measurements.
- Reconstruct γ and q from $\mathcal{E}_\gamma$ and $\mathcal{E}_q$.
- Nonlinear PDE (the modified 0–Laplacian)

$$\begin{cases} \nabla \cdot \left(\dfrac{\mathcal{E}_\gamma}{|\nabla u|^2} \nabla u \right) + k^2 \dfrac{\mathcal{E}_q}{|u|^2} u = 0 & \text{in } \Omega\ , \\ \dfrac{\mathcal{E}_\gamma}{|\nabla u|^2} \dfrac{\partial u}{\partial \nu} = g & \text{on } \partial\Omega\ . \end{cases}$$

Multi-physics Imaging

Reconstruct the electromagnetic parameters knowing the electromagnetic internal energies:

- Linearized versions of the nonlinear (zero-Laplacian) PDE problems.
- Optimal control approach: minimize over the electromagnetic parameters the discrepancy between the computed and reconstructed internal energies.
- Optimal control approach: more efficient approach specially with incomplete internal measurements of the electromagnetic energy densities.
- Resolution of order the size of the focal spot + stability (wrt measurement noise).

Conclusion

- Expansion methods: power strategy for increasing stability and resolution.
- Expansion methods: combine a variety of mathematical and computational tools.
- Extension to elasticity (concept of elastic moment tensor and viscous moment tensor, inner expansions for elastography, weighted Helmholtz decomposition for time reversal imaging).
- (with H. Kang, Expansion Methods, Handbook of Mathematical Methods in Imaging, Ed. O. Scherzer, Springer, 2011.)
- Expansion methods: story has still long way to go!